Supplementary Information (SI) for Lab on a Chip.

Bioinspired Quality-Based Sperm Sorting in a Spiral Microfilter-Enhanced Microfluidic: Enhancing DNA Integrity via Rheotaxis and Boundary Dynamics

Donya Shahhoseini[a] , Naser Naserifar[a,*]

[a] Department of Mechanical Engineering, K. N. Toosi University of Technology, Tehran, Iran.

*Corresponding author, Email: naserifar@kntu.ac.ir

1. Supplementary Justification of Model and Methods

The use of bovine sperm in this study serves as a reliable model for initial validation, leveraging conserved rheotaxis and thigmotaxis behaviors shared with human sperm, as demonstrated in previous studies[1,2]. The larger head size of bovine sperm (~9 µm compared to ~4.5 µm for human sperm) may influence thigmotaxis dynamics; however, the similarity in boundary interaction behaviors supports the potential applicability of the device to human assisted reproductive technologies (ART). The selection of Phosphate-Buffered Saline (PBS) as a buffer, effective for short-term sorting within 20 minutes, maintains high motility (96.60%) and viability (98.02%) without inducing premature capacitation, consistent with findings from prior microfluidic sperm sorting research[3,4].Cryopreserved bovine sperm were chosen for their standardized availability and reproducibility, demonstrating robust performance across diverse semen qualities, including oligospermia. This supports the device's potential relevance to clinical settings, where cryopreserved human sperm are commonly utilized.

2. Microscopic Imaging and Video Capture

Sperm samples were imaged and recorded using a Nikon Eclipse TS100 inverted microscope at a frame rate of 30 frames per second. The analysis adhered to the guidelines established by the World Health Organization (WHO)[5] and included assessments of sperm motility, concentration, viability, and genetic integrity. Sperm motility trajectories were processed using the openCASA module, an open-source plugin within ImageJ. Additional data analysis was conducted using a custom Python script. Key sperm motility parameters, including VCL, VAP, VSL and LIN were computed and rigorously evaluated to ensure comprehensive motility analysis.

3. Sperm Concentration Test

Sperm concentration is a crucial determinant of semen quality and directly influences the success of assisted reproductive techniques such as IUI and IVF. To measure sperm concentration, a Neubauer hemocytometer was employed. The grid on this slide consists of nine large squares, each further divided into smaller squares. A sperm sample was diluted

at a 1:20 ratio with PBS solution to ensure accurate counting, and 10 μL of this dilution was pipetted beneath a 22×22 mm cover slip, forming a uniform depth of 1 mm. Using a microscope, the central square (square 5) was selected for analysis. This square, containing five horizontal rows with a total volume of 20 nL per row, was examined systematically. Counting began from the first row, continuing until 200 sperm were recorded. If fewer than 200 sperm were present in one row, subsequent rows were included. Sperm heads and tails were both counted, adhering to the convention of including two specific boundary lines. Finally, the number of sperm counted in the central square was divided by the number of rows to determine the concentration in millions per mL which was then multiplied by the total sample volume to calculate the final sperm count.

4. SCMA (Sperm Chromatin Maturity Assay) Test

SCMA test is designed to assess the maturity of sperm chromatin and its genetic quality[6]. This test examines the structure and packaging of chromatin within the sperm nucleus, playing a crucial role in preserving DNA integrity and the fertility potential of sperm. Initially, the sperm sample is diluted with PBS buffer to achieve a concentration of 10 million sperm per mL. The sperm suspension is then smeared onto a microscope slide and allowed to dry for a designated period. Subsequently, the slide is fixed in a fixative (70% ethanol) for 30 minutes, followed by a 5-minute immersion in Aniline dye. After a simple wash, the slide is immersed in eosin for 3 minutes. Finally, the sample is analyzed under a light microscope with a 1000x magnification, where 200 sperm are evaluated. Only sperm that clearly show both a head and tail are selected for analysis. Sperm with a dark blue head are identified as immature, whereas sperm with a pink head are considered mature.

5. Statistical Data

Statistical analysis in this study was performed using two methods: the two-sample t-test and one-way analysis of variance (ANOVA). The two-sample t-test was employed to compare the means of two independent groups to assess significant statistical differences between them. For comparisons involving more than two groups, one-way ANOVA was used. When significant differences were detected in ANOVA, Tukey's HSD test was applied as a post-hoc analysis to identify specific group differences. Data were reported as mean ± standard deviation (Mean ± SD), and statistical analyses were conducted using GraphPad Prism version 10.4.1.627. A p-value of < 0.05 was considered statistically significant. In this study, the data collection criterion was based on the position of the sperm at the moment of entry into the channel branches, rather than solely relying on the sperm collected in the central section of the channel. This decision was made due to operational limitations in collecting sperm from the central section. Due to repeated testing, a significant number of sperm would enter this section, which, due to the channel design features and microfluidic flows, were not easily washable or separable. This limitation was identified as a challenge in the research process, and as a result, it was decided that data would be collected based on the sperm's position at the time of entry into the branches to prevent the influence of this issue and improve the accuracy of the separation process. The figure illustrates the movement pathways of sperm within the microfluidic channel, plotted using velocity-averaged paths (VAP). In this image, Grade A and B sperm are primarily

directed toward branch 1 or 2, while some Grade A sperm, after colliding with the dividing walls, altered their direction and moved into the next zone. Additionally, Grade C and D sperm were predominantly washed out of the channel due to the influence of recirculating flow. The positions of the branches and key separation regions are highlighted in the figure.

6. Supplementary figure:

Fig. S1: Illustrates the smoothed tracking paths (VAP) of 10 sperm in zone 1 as they enter the separation zone. The figure highlights the distinct trajectories of sperm grades A, B, C, and D, with their X and Y positions plotted in pixels (ranging from 0 to 900 µm for X and 200 to 1200 µm for Y). Grade A and B sperm (e.g., Sperm 1, 3, 5, 6, 8) are shown migrating toward branches 1 or 2 near the outlet (around Y = 900–1200 µm), exhibiting redirection behavior. Specifically, grade A sperm such as Sperm 2 and Sperm 7 deviate from the main path upon colliding with the branch separators, redirecting toward zone 2 instead of entering the outlet branches. In contrast, grade C and D sperm (e.g., Sperm 4, 9, 10) are washed back toward the reservoir, converging in a region with X-coordinates between 0–570 µm and Y-coordinates between 900–1300 µm, as indicated by the circular annotations.

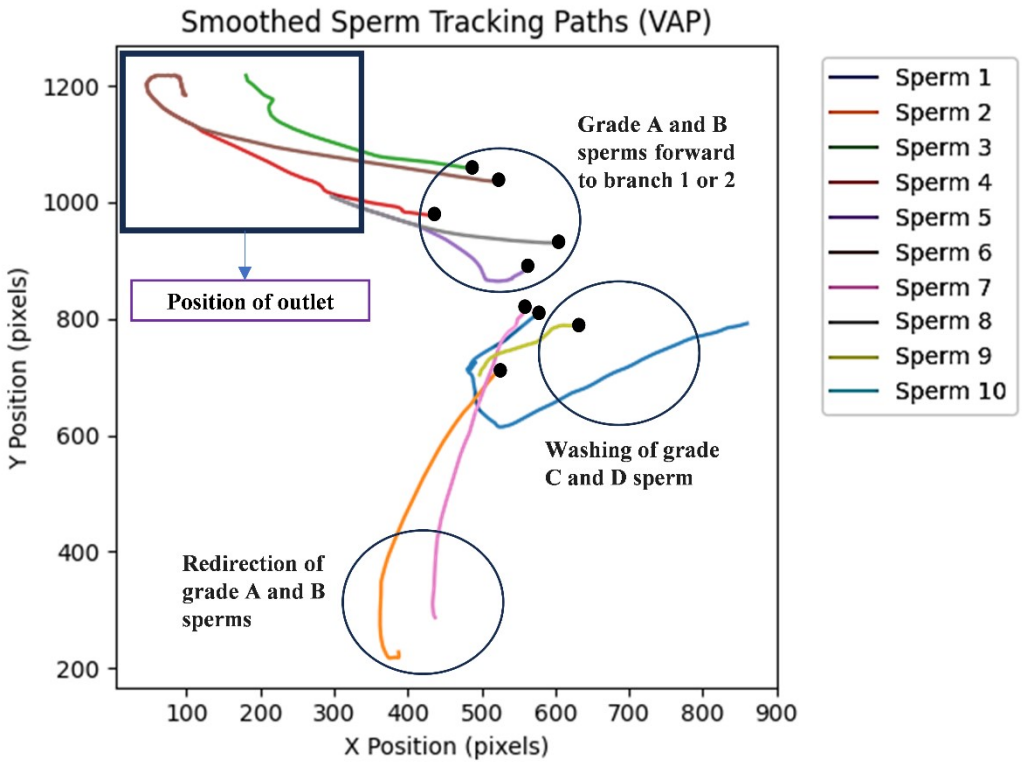

Fig. S2: Smoothed sperm tracking path in zone1: the trajectories of 10 grade A sperm are illustrated. These sperm entered the separation zone (the inlet area of the bifurcations) with varying head orientations and straight-line movement. They were guided toward the outlet coordinates with the assistance of the channel boundaries. Each color represents a

different sperm, following its own unique path within the channel, with the black dots indicating the starting points of the sperm movement.

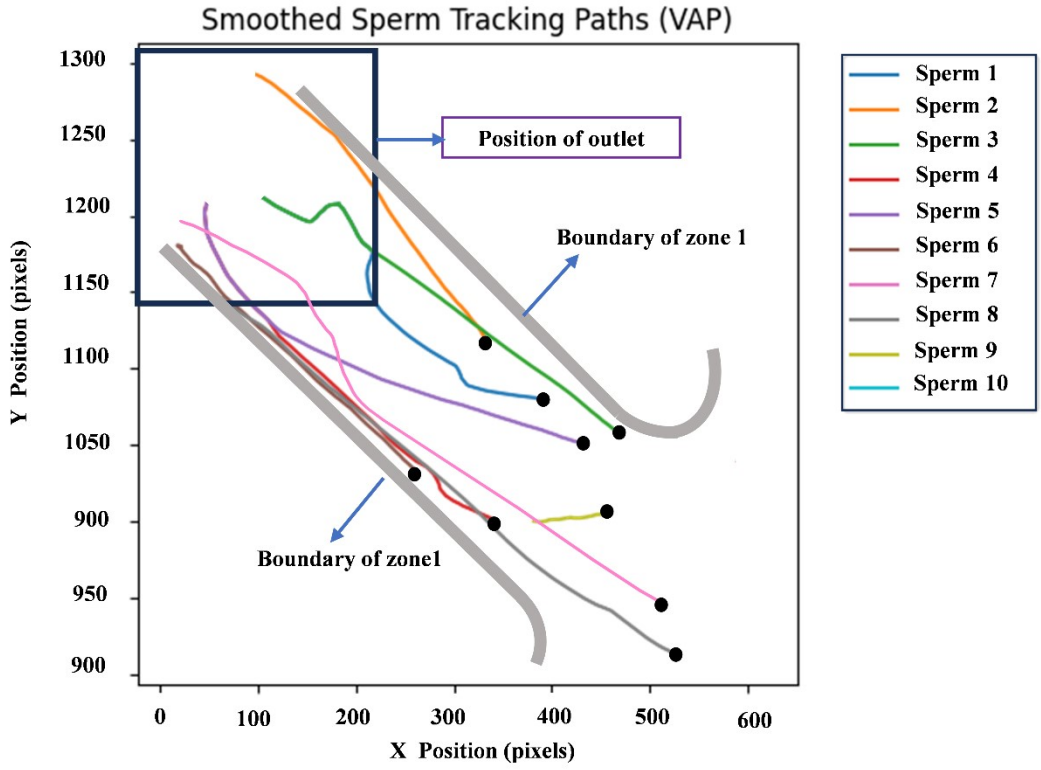

7. Supplementary Tables:

Table S1 compares bovine and human sperm:

Characteristic	Bovine Sperm	Human Sperm	Source
Head Length	~ 8.99 ± 0.06 µm	~4.5–4.9 µm	[5,7,8]
Head Width	~4–6 µm	~3.1–3.5 µm	[5,7,9]
Motility (Grade A VSL)	≥25 µm s^{-1}	≥25 µm s^{-1}	[5,10]
Rheotaxis Behavior	Strong	Strong	[1,11]
Thigmotaxis	Pronounced boundary-following	Pronounced boundary-following	[12]
DNA Fragmentation	~17% (Fig. 10c)	15–30% (infertile samples)	[13,14]
Device Validation	95% classification	Planned	This study

Table S2 compares microfluidic sperm-sorting devices:

Device	Principle	Structure	Throughput	Cost	Clinical Validation	Performance (vs. Article 10)	Limitations	Source

Bio- inspired microchannel	Rheotaxis, boundary-following, butterfly motion	Parallel channels, 180 µm sorting channel with UTJ-like constrictions	50 µL in 30 min	Low	No explicit validation	Lower motility (VSL: 63.4–74 µm/s vs. 149 µm/s), similar DFI (2.3–3.7% vs. 3.58%), similar vitality (100% vs. 98.02%)	Limited to specific flow rates, reduced yield at high flows	13
Boomerang-shaped microchannel	Rheotaxis, boundary-following	Boomerang-shaped microchannels, 500 µm side channels	>16,000 sperm in <20 min	Low	No explicit validation	Similar motility (96% vs. 96.6%), lower SDF (~3% vs. 3.58%), no SCI data	Reduced efficiency at high sperm concentrations, potential sperm loss	14
Butterfly-shaped microchannel	Rheotaxis, boundary-following	Butterfly-shaped channels, 250–300 µm wide, 60° arrays	19,700–25,500 sperm in 20 min	Low	Compared with SU	Similar motility (95.9% vs. 96.6%), lower SDF (vs. 3.58%), lower viability (97.8% vs. 98.02%)	Sensitivity to flow rate variations, requires large sample volumes	15
Micropocket geometries-based-microchannel	Rheotaxis, boundary-following	1.5 mm channel, oval micropockets	15,480 sperm in 20 min	Low	No explicit validation	Higher motility (100% vs. 96.6%), lower VCL (128 µm/s vs. 181.27 µm/s), no SDF/SCI data	Micropocket saturation limits yield, complex retrieval process	16
Microfluidic corral system	Rheotaxis, boundary-following	500 µm channel, seven corrals	150–600 sperm/corral in 2 min	Low	No explicit validation	Higher motility (100% vs. 96.6%), lower velocity (51–82 µm/s vs. 149 µm/s), no SDF/SCI data	Low throughput, limited scalability for clinical use	1
Acoustofluidic chip	Bulk acoustic waves	PDMS chip, horseshoe structures, PZT transducer	~11,000 sperm in <10 min	High	No explicit validation	Lower motility (+50% vs. 96.6%), higher DFI (22% vs. 3.58%), lower viability (+44% vs. 98.02%)	Requires precise bubble control, reduced yield at high voltages	17
IDEP microdevice	Dielectrophoresis	Glass channel, cylindrical posts	10 µL in 30–60 s	High	No explicit validation	Lower viability (>75% vs. 98.02%), no motility/SDF/SCI data	High voltages impair cell viability, short processing window	18
Thermoseparation device	Thermotaxis	Lucite tube, 40 µm pores	30–50 million sperm/mL in 15–20 min	Low	No explicit validation	Lower velocity (VCL: 70–85 µm/s vs. 181.27 µm/s), no SDF/SCI/viability data	Low yield due to small capacitated fraction, complex gradient setup	19
Flow-free microfluidic	Chemotaxis	Hybrid hydrogel chip, 350 µm channels	0.5 µL in ~20 min	Low	No explicit validation	No motility/SDF/SCI data, lower viability decline (0.7%/min vs. 98.02%)	Slow gradient formation, limited to short-range chemotaxis	20
Spiral microfilter microfluidic	Rheotaxis, thigmotaxis, boundary detachment	PDMS spiral channel, 250 µm wide, 12 branches	6.3 million sperm/mL in 20 min	Low	Compared with SU, DGC	Motility: 96.6%, Viability: 98.02%, SDF: 3.58%, SCI: 3.19%, VCL: 181.27 µm/s, VSL: 149 µm/s, LIN: 82.22%	High sperm concentration reduces efficiency, complex fabrication process	This study

Table S3 compares our device with clinical methods:

Method	Principle	Throughput (Total motility)	Recovery Rate	DNA Integrity	Cost	Technical Requirements	Limitations
This Study	Rheotaxis, thigmotaxis	~95%	~95%	84.09% less damage vs. DGC	Low	Cleanroom, microfluidic setup	Longer processing time, lower recovery
Swim-up	Motility-based	~63%	~58%	Moderate damage	Low	Basic lab setup	No oligospermia compatibility, single-grade
DGC	Density-based	~74%	~69%	High damage	Moderate	Centrifuge, gradient media	Centrifugation stress, two-grade

8. Supplementary movies:

Movie S1: Visualizes sperm separation dynamics under a backflow rate exceeding 100 nL min^{-1}. The movie highlights grade A sperm exhibiting rheotaxis and thigmotaxis, with most being washed away by the high backflow upon reaching the central region of the channel. Only those migrating toward the channel walls and displaying thigmotaxis successfully enter the outlet branches.

Movie S2: Depicts the flushing of grade C and D sperm under backflow rates exceeding 100 nL min^{-1} and between 50–100 nL min^{-1}. The movie shows these sperm being effectively washed out by the backflow, preventing their progression to the outlet branches.

Movie S3: Illustrates sperm separation under a backflow rate between 50–100 nL min^{-1}. The movie showcases grade A and B sperm exhibiting rheotaxis, thigmotaxis, and boundary detachment-reattachment behaviors due to the gradually decreasing backflow. Separation of these sperm occurs primarily in zones 1 and 2.

Movie S4: Shows sperm separation dynamics under a backflow rate below 50 nL min^{-1}. The movie focuses on grade C sperm swimming against the flow, demonstrating rheotaxis but lacking clear thigmotaxis or boundary detachment-reattachment behaviors. These sperm follow irregular, oscillatory paths, reaching zone 3.

Movie S5: Depicts grade A sperm in zone 1, navigating along channel boundaries via rheotaxis, thigmotaxis boundary detachment-reattachment behaviors. The sperm detach at varying angles upon encountering the upper boundary, migrating toward Branch 1 and Branch 2, guided by the channel's curvature and backflow adjustment.

Movie S6: Captures grade B sperm in zone 1, following the spiral channel's path via rheotaxis without boundary detachment-reattachment. Some sperm redirect toward Branch 1 and Branch 2 upon colliding with branch separator walls, influenced by the channel's curvature.

Movie S7: Shows grade C and D sperm in zone 1, carried back to the sperm reservoir by the prevailing backflow, highlighting their inability to resist hydrodynamic forces and reach the outlet branches.

Movie S8: Visualizes grade A sperm in zone 2, maintaining rheotaxis and thigmotaxis under a lower, stable backflow rate, following paths similar to those in zone 1 and migrating toward outlet branches.

Movie S9: Displays grade B sperm in zone 2, exhibiting enhanced rheotaxis and thigmotaxis due to reduced backflow. Most are directed to outlet branches, with grade C and D sperm flushed out.

Movie S10: Illustrates grade B sperm in zone 3, utilizing slower backflow to exhibit thigmotaxis and boundary detachment-reattachment, enabling migration to outlet branches.

Movie S11: Shows grade C sperm in zone 3, following oscillatory paths with reduced backflow, shifting along boundaries to reach outlet branches, with some progressing to zone 4.

Movie S12: Captures grade D sperm in zone 3, primarily flushed out by backflow, though a few enter the channel alongside grade C sperm, highlighting their limited motility.

Movie S13: Depicts grade C and D sperm in zone 4, with grade C sperm navigating oscillating paths to outlet branches and grade D sperm entering branches as backflow significantly decreases.

Movie S14: Visualizes sperm concentration in the first region of the microfluidic channel, where the average sperm concentration peaks at 3.52 ± 0.25 million sperm per milliliter. The film highlights significant sperm accumulation, establishing this area as the primary zone of concentration, driven by initial hydrodynamic conditions and sperm behavior (corresponding to Fig. 8b, Fig. 9a).

Movie S15: Depicts sperm concentration in the second region, with an average concentration of 1.43 ± 0.15 million sperm per milliliter. The film shows a notable reduction in sperm density compared to the first region, reflecting the influence of progressing flow dynamics through the spiral channel (corresponding to Fig. 8b, Fig. 9b).

Movie S16: Illustrates sperm concentration in the third region, where the average concentration drops to 0.98 ± 0.11 million sperm per milliliter. The film captures the lowest concentration among the earlier zones, attributed to hydrodynamic variations and sperm washout due to backflow (corresponding to Fig. 8b, Fig. 9c).

Movie S17: Shows sperm concentration in the fourth region at the channel's exit, with a minimum average concentration of 0.31 ± 0.02 million sperm per milliliter. The film underscores the substantial decline in sperm density, driven by the interplay of channel hydrodynamics and sperm responses to regional flow conditions (corresponding to Fig. 8b, Fig. 9d).

9. References

1. Zaferani M, Cheong SH, Abbaspourrad A. Rheotaxis-based separation of sperm with progressive motility using a microfluidic corral system. Proceedings of the National Academy of Sciences. 2018;115(33):8272-8277.

2. Yaghoobi M, Azizi M, Mokhtare A, Javi F, Abbaspourrad A. Rheotaxis quality index: a new parameter that reveals male mammalian in vivo fertility and low sperm DNA fragmentation. *Lab on a Chip*. 2022;22(8):1486-1497.

3. Katigbak RD, Dumée LF, Kong L. Isolating motile sperm cell sorting using biocompatible electrospun membranes. *Scientific Reports*. 2022;12(1):6057.

4. Mane NS, Puri DB, Mane S, Hemadri V, Banerjee A, Tripathi S. Separation of motile human sperms in a T-shaped sealed microchannel. *Biomed Eng Lett*. 2022;12(3):331-342.

5. Organization WH. *WHO Laboratory Manual for the Examination and Processing of Human Semen*. World Health Organization; 2021. Accessed January 31, 2025.

6. Dutta S, Henkel R, Agarwal A. Comparative analysis of tests used to assess sperm chromatin integrity and DNA fragmentation. *Andrologia*. 2021;53(2). doi:10.1111/and.13718

7. Esteves SC, Roque M, Bedoschi G, Haahr T, Humaidan P. Intracytoplasmic sperm injection for male infertility and consequences for offspring. *Nature Reviews Urology*. 2018;15(9):535-562.

8. Valverde A, Barquero V, Soler C. The application of computer-assisted semen analysis (CASA) technology to optimise semen evaluation. A review. *Journal of Animal and Feed Sciences*. 2020;29(3):189-198.

9. Yazdan Parast F, O'Bryan MK, Nosrati R. Sperm Syringe: 3D Sorting Platform for Assisted Reproduction. *Adv Materials Technologies*. 2022;7(9):2101291. doi:10.1002/admt.202101291

10. Yaghoobi M, Azizi M, Mokhtare A, Abbaspourrad A. Progressive bovine sperm separation using parallelized microchamber-based microfluidics. *Lab on a Chip*. 2021;21(14):2791-2804.

11. Miki K, Clapham DE. Rheotaxis guides mammalian sperm. *Current Biology*. 2013;23(6):443-452.

12. Ahmadkhani N, Saadatmand M, Kazemnejad S, Abdekhodaie M. Qualified sperm selection based on the rheotaxis and thigmotaxis in a microfluidic system. *Biomed Eng Lett*. 2023;13(4):671-680.

13. Tabalvandani MB, Javadizadeh S, Badieirostami M. Bio-inspired progressive motile sperm separation using joint rheotaxis and boundary-following behavior. *Lab on a Chip*. 2024;24(6):1636-1647.

14. Zeaei S, Targhi MZ, Halvaei I, Nosrati R. High-DNA integrity sperm selection using rheotaxis and boundary following behavior in a microfluidic chip. *Lab on a Chip*. 2023;23(9):2241-2248.

15. Asl AS, Targhi MZ, Zeaei S, Halvaei I, Nosrati R. High-throughput selection of sperm with improved DNA integrity and rapidly progressive motility using a butterfly-shaped chip compared to the swim-up method. *Lab on a Chip*. 2024;24(20):4907-4917.

16. Sarbandi IR, Lesani A, Moghimi Zand M, Nosrati R. Rheotaxis-based sperm separation using a biomimicry microfluidic device. *Scientific reports*. 2021;11(1):18327.

17. Saeidpour Z, Bouloorchi Tabalvandani M, Javadizadeh S, Badieirostami M. Enhanced sperm isolation via bulk acoustic waves for high-throughput motility screening. *Scientific Reports*. 2024;14(1):26717.

18. Rosales-Cruzaley E, Cota-Elizondo PA, Sánchez D, Lapizco-Encinas BH. Sperm cells manipulation employing dielectrophoresis. *Bioprocess Biosyst Eng*. 2013;36(10):1353-1362.

19. Bahat A, Caplan SR, Eisenbach M. Thermotaxis of Human Sperm Cells in Extraordinarily Shallow Temperature Gradients Over a Wide Range. *PLOS ONE*. 2012;7(7):e41915.

20. Berendsen JTW, Kruit SA, Atak N, Willink E, Segerink LI. Flow-Free Microfluidic Device for Quantifying Chemotaxis in Spermatozoa. *Analytical Chemistry*. 2020;92(4):3302-3306.